A Robust Uniform Control Approach for VTOL Aircraft

Jacob Cook
Research Engineer
Dynamic Systems and Control Branch
NASA Langley Research Center
Hampton, VA, U.S.A.

Irene Gregory
Senior Technologist
Dynamic Systems and Control Branch
NASA Langley Research Center
Hampton, VA, U.S.A.

ABSTRACT

We present a uniform control approach for transitioning vertical take-off and landing aircraft. The approach combines several well-understood linear techniques, including robust servomechanism linear quadratic regulation, control allocation, and gain scheduling, to provide a practical control framework that can be used to unify the control design process in all flight regimes. The choice of command variables provides a pilot/operator with a uniform set of intuitive control inputs through all phases of flight while also being easily integrated into autonomous trajectory tracking operations. The control method is applied to the NASA LA-8 aircraft, a tandem tiltwing distributed electric propulsion research vehicle designed at NASA Langley Research Center. The trim envelope of the aircraft is explored and the aircraft control authority analyzed throughout the transition corridor. The uniform control approach is then used to develop reference command tracking controllers for both the longitudinal and lateral-directional dynamics. An example trajectory is simulated to demonstrate how the controller effectively transitions the aircraft from hover to forward flight and vice versa while tracking a desired trajectory.

INTRODUCTION

Urban Air Mobility (UAM) operations are based on vertical take-off and landing (VTOL) aircraft, some of which, transition from a rotor or thrust- borne-flight to a more efficient wing- or lift-borne flight. Transitioning UAM vehicles tend to fall into one of the three general classes of VTOL configurations: tiltwing, where the wing and propulsion rotate as a unit from a vertical to horizontal position; a tiltrotor, where the wing is fixed and the propulsion units rotate between a vertical and horizontal position; or lift+cruise, where both the wings and propulsion units are fixed and there are separate propulsors that provide lift in hover and thrust in forward flight. Common across all these platforms is the use of propulsion units and aerodynamic surfaces as control actuators. Their combination in different flight regimes provides redundancy in control force and moment generation; however their individual effectiveness and energy requirements vary as the flight envelope is traversed.

Transitioning VTOL aircraft must operate in three general flight modes: hover, forward flight, and transition. Hover and forward flight are well understood flight regimes but operationally present two very distinct modes of flight. Transition, a less well understood regime, must seamlessly stitch the two flight modes together, taking into account the changing aerodynamics of the aircraft as well as the dynamic nature of control force and moment production from available actuators.

The combination of the transitioning aerodynamics and control actuation make VTOL aircraft, in general, very complex. Compounding these complexities is the plethora of configurations being proposed for the UAM market, each with their own unique aerodynamic properties and available control effectors. From the outset, it is easy to see that an automatic control system is needed to improve vehicle flyability and provide foundational capabilities to build on as we transition to autonomous operations.

Traditional fly-by-wire systems made use of robust linear methods to develop control and stabilization algorithms for conventional aircraft (Refs. 1–4). Because of the broad range of flight conditions at which a VTOL aircraft are expected to operate, various different approaches have been proposed and implemented. In (Refs. 5, 6), a velocity control concept is proposed that makes use of a cascaded loop architecture. Redundant controls are abstracted through the use of virtual control effectors and feed forward commands are provided by a predefined trim envelope. The F-35 control law (Refs. 7, 8) uses an on board model of the aircraft aerodynamic and propulsion characteristics and a control allocation methodology (cascaded generalized inverse algorithm) to provide rate control of the aircraft in all phases of flight. A nonlinear dynamic inversion approach is taken in (Refs. 9–11) where the changing relative degree of the control inputs are handled by introducing the pitch and roll angle as virtual controls. Additionally, the heading frame velocities are used to provide a common set of control commands throughout the flight envelope.

This paper presents a Robust Uniform Control Architecture for VTOL aircraft. The main contribution being a configuration-independent framework which unifies the control design across all flight regimes and thus provides a uniform set of control commands throughout the entire flight en-

Presented at the VFS Autonomous VTOL Technical Meeting and Electric VTOL Symposium, January 26–28, 2021.

velope.

The control architecture builds upon the foundational principles of Robust Servomechanism Linear Quadratic Regulator (RSLQR) control theory, but formulates the problem using general accelerations as the commanded input. The desired control accelerations are mapped to the set of physical and virtual control inputs by way of a weighted pseudo-inverse. The formulation enables a consistent control strategy over the entire operating envelope of a VTOL aircraft.

The effectiveness of the Robust Uniform Controller is demonstrated in simulation using a model of NASA Langley's LA-8 tandem tiltwing research aircraft (Ref. 12). A Trajectory tracking maneuver, that transitions the aircraft from hover to forward flight and back to hover, is demonstrated.

AIRCRAFT DESCRIPTION AND AERODYNAMIC MODEL

The Langley Aerodrome No. 8 (LA-8) is a distributed electric propulsion, VTOL aircraft designed and built at the NASA Langley Research Center (Ref. 12). The aircraft, shown in figure 1, is a tandem tiltwing with four propellers mounted along the leading edge of each wing. The wings rotate, from the zero degree fixed-wing position, a full 90 degrees such that the wing and propeller thrust axis is vertical. The wing tilting mechanisms operate independently of one another such that the wings may be at different tilt angles simultaneously. Each wing has a set of flaps located on the inner portion of the wing and a set of elevons on the outer portion. These are shown in figure 2. An inverted V-tail at the rear of the aircraft includes a set of ruddervator surfaces. Each surface may be operated independently. The propellers of the LA-8 are speed controlled and are also commanded independently. The direction of rotation of the propellers alternates as indicated in figure 2.

Figure 1. LA-8 aircraft undergoing wind tunnel testing

The aerodynamic model of the LA-8 was developed over multiple wind tunnel experimental runs. The initial wind tunnel test used a one-factor-at-a-time approach to explore the transition corridor by trimming the aircraft at different wing tilt angles (Ref. 13), effectively mapping out an expected flight envelope. The subsequent test runs used Design of Experiments (DOE) methods to build a high-fidelity 23-factor model that captures the many interactive effects of this complex aircraft (Ref. 14). Additional isolated propeller testing was performed to determine the propeller performance through a broad range of incidence angles and capture the deviations in thrust and torque generation, as well as the off axis forces and moments generated when subject to flow at a high incidence angle (Ref. 15).

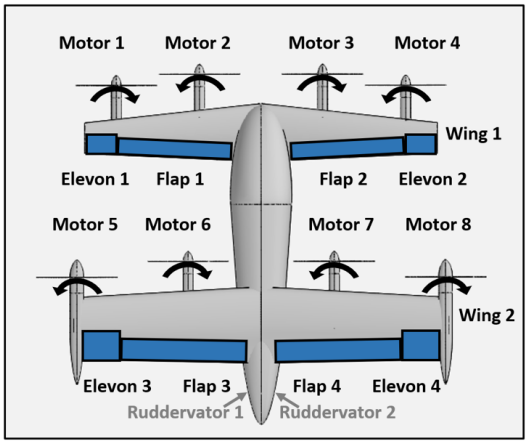

Figure 2. Control surface and rotor diagram of the LA-8

The resulting six-degree-of-freedom model provides the aeropropulsive forces and moments over a range of flight conditions from hover to forward flight centered around a body level flight condition. Of note, the model contains asymmetries discovered while testing, among them, is a difference in thrust production of the clockwise and counterclockwise propellers, attributed to the different manufacturing processes by which they were obtained. Since the wind tunnel model is also the flight vehicle, there was no attempt to symmetrize the model; the asymmetries, are therefore present in this presentation. Additionally, while testing at higher dynamic pressures (5 PSF) the elevon servos burned out causing the model to reflect diminished control authority of these actuators in forward flight. Due to extenuating circumstance (COVID-19 pandemic), additional wind tunnel testing could not be performed to rectify the elevon measurements. Therefore, the artificial control reduction remains in the model and provide an effective example of how the control architecture allows the designer to easily distribute control actuation to other available effectors.

REFERENCE FRAMES

Three reference frames are used throughout this study: the inertial North-East-Down (NED) frame, the aircraft body frame, and the heading frame. The aircraft body frame is defined with the origin at the nominal center of mass with the x-axis pointing out the nose, y-axis out the right wing, and z-axis completes the right hand rule. The rotation from body frame to the inertial frame is parameterized by the Euler angles,

$\eta = [\phi, \theta, \psi]^T$, (roll, pitch, and yaw respectively). The rotation matrix $R \in SO(3)$ is defined as

$$R = [R_x(\phi)R_y(\theta)R_z(\psi)]^T \tag{1}$$

where $R_x(\cdot)$, $R_y(\cdot)$, and $R_z(\cdot)$ are the intermediate single-axis rotation matrices, explicitly defined as

$$R_x(x) = \begin{bmatrix} 1 & 0 & 0 \\ 0 & \cos x & \sin x \\ 0 & -\sin x & \cos x \end{bmatrix} \tag{2}$$

$$R_y(x) = \begin{bmatrix} \cos x & 0 & -\sin x \\ 0 & 1 & 0 \\ \sin x & 0 & \cos x \end{bmatrix} \tag{3}$$

$$R_z(x) = \begin{bmatrix} \cos x & \sin x & 0 \\ -\sin x & \cos x & 0 \\ 0 & 0 & 1 \end{bmatrix}. \tag{4}$$

The heading frame is defined as the inertial frame rotated about the z-axis by the heading angle ψ, with the origin coincident with the aircraft center of mass. The rotation from body frame to the heading frame is defined as the abbreviated rotation $\bar{R} = [R_x(\phi)R_y(\theta)]^T$. A vector expressed in the body frame is mapped to the heading frame through the transformation $\bar{\mathrm{v}} = \bar{R}\mathrm{v}_b$, where the subscript b denotes a vector expressed in the body frame, whereas the over-bar indicates the heading frame.

GUIDANCE COMMANDS

Flight maneuvers of a transitioning VTOL aircraft are expected to encompass those of rotor-craft in addition to conventional flight. This includes stationary hover, and pure lateral and vertical maneuvers. For this reason, typical aircraft guidance commands, such as airspeed, flight path angle, and heading angle, are inadequate to capture the full operating range, particularly in hover where the flight path angle is undefined at zero total velocity.

Additionally, UAM aircraft are expected to operate in highly congested airspace. To ensure vehicle separation, both spatial and temporal adherence to a scheduled trajectory is necessary. Therefore, inertially referenced speeds, such as ground speed, are used to describe a desired trajectory (Ref. 16).

The use of heading frame coordinates to describe the desired trajectory provides a set of guidance commands that can be used to describe the full range of maneuvers of a VTOL aircraft. The desired heading frame velocity vector $\bar{\mathrm{v}}_d = [\bar{u}_d, \bar{v}_d, \bar{w}_d]^T$, is comprised of two horizontal components, $\bar{u}_d$ and $\bar{v}_d$, and the vertical component $\bar{w}_d$. The forward and vertical components, $\bar{u}_d$ and $\bar{w}_d$, are analogous to the total velocity and flight path angle, but do not suffer from the same ill conditioning when the velocity goes to zero. Additionally, as the forward velocity increases the vertical velocity command may remain constant when performing, for instance, a transition with a constant climb rate. In contrast, commands constructed of total speed and flight path angle would necessitate both commands changing in concert, which may further complicate the feedback control design and degrade the performance of the system.

A purely lateral maneuver, such as sideways flight in hover, is commanded using the lateral component of the velocity in the heading frame, $\bar{v}_d$. Turning flight and stationary yaw maneuvers are incorporated into the guidance commands by including the desired turn rate $\dot{\psi}_d$ such that the complete guidance command is comprised of the desired heading frame velocity and turn rate, $r(t) = [\bar{\mathrm{v}}_d^T(t), \dot{\psi}_d(t)]^T$.

The formulation of the guidance commands in the heading frame provides seamless integration into existing trajectory generation tools, in which smooth, four-dimensional trajectories may be decomposed into the four guidance components. Additionally, the heading frame commands provide an intuitive set of uniform control inputs for a pilot or operator to direct the aircraft in all phases of flight.

AIRCRAFT DYNAMICS

The angular kinematics of the vehicle are expressed as the time derivatives of the Euler angles

$$\dot{\eta} = S\omega, \tag{5}$$

where ω is the angular rate of the aircraft expressed in the body frame with components (p, q, r) and S is the non-orthogonal transformation from the body angular rates to the time derivatives of the Euler angles

$$S = \begin{bmatrix} 1 & \sin\phi\tan\theta & \cos\phi\tan\theta \\ 0 & \cos\phi & -\sin\phi \\ 0 & \sin\phi/\cos\theta & \cos\phi/\cos\theta \end{bmatrix}. \tag{6}$$

Because we seek to track heading frame velocities, $\bar{\mathrm{v}} = [\bar{u}, \bar{v}, \bar{w}]^T$, it makes sense to formulate the translational dynamics in the heading frame as

$$\dot{\bar{\mathrm{v}}} = -\dot{\psi}\hat{e}_3 \times \bar{\mathrm{v}} + g + \frac{1}{m}\bar{F}(\bar{\mathrm{v}}, \omega, \bar{R}, u), \tag{7}$$

where $\bar{F}(\cdot)$ is the aero-propulsive forces acting on the aircraft expressed in the heading frame, $g = [0, 0, a_g]^T$ is the gravitational acceleration vector, u is the vector of available control effectors, and $\hat{e}_3$ is the unit vector in the body z-direction. Expanding (7) gives

$$\begin{pmatrix} \dot{\bar{u}} \\ \dot{\bar{v}} \\ \dot{\bar{w}} \end{pmatrix} = \begin{pmatrix} \dot{\psi}\bar{v} + \frac{1}{m}\bar{X}(\bar{\mathrm{v}}, \omega, \bar{R}, u) \\ -\dot{\psi}\bar{u} + \frac{1}{m}\bar{Y}(\bar{\mathrm{v}}, \omega, \bar{R}, u) \\ a_g + \frac{1}{m}\bar{Z}(\bar{\mathrm{v}}, \omega, \bar{R}, u) \end{pmatrix}. \tag{8}$$

The rotational dynamics are given by

$$J\dot{\omega} = -\omega \times J\omega + \tau(\bar{\mathrm{v}}, \omega, \bar{R}, u) \tag{9}$$

where J is the inertia matrix, and τ is the aero-propulsive moments expressed in the body frame. Expanding (9) gives the following set of equations for the rotational dynamics:

$$\begin{bmatrix} \dot{p} \\ \dot{q} \\ \dot{r} \end{bmatrix} = J^{-1}\left(\begin{bmatrix} J_yrq - J_{xz}qp - J_zqr \\ J_xp^2 - J_zr^2 \\ J_xqp + J_{xz}qr - J_ypq \end{bmatrix} + \begin{bmatrix} L(\bar{\mathrm{v}}, \omega, \bar{R}, u) \\ M(\bar{\mathrm{v}}, \omega, \bar{R}, u) \\ N(\bar{\mathrm{v}}, \omega, \bar{R}, u) \end{bmatrix}\right). \tag{10}$$

EQUILIBRIUM MANIFOLD EXPLORATION

The equilibrium manifold is the set of states at which the aircraft is in a constant operating (trim) condition. The trajectories described by the equilibrium manifold are the set of constant radius helical trajectories which includes level flight and steady level turns. For transitioning aircraft, exploring the equilibrium manifold provides valuable insight into how the aircraft might fly including: how the effectiveness of the of the control surfaces varies throughout the envelope, how the lifting force is distributed between the lifting rotors and the wing, and at what speeds the aircraft is fully transitioned to wing-borne flight. The trim points, at select conditions in the flight envelope, provide the basis for control design, as well as feed forward actuation and pitch and roll commands as a function of the aircraft's desired speed, climb rate and turn rate.

The aircraft is said to be in equilibrium (or trimmed) when the translational and rotational dynamics as well as the derivatives of the pitch and roll angles are equal to zero ($\dot{\bar{\mathrm{v}}} = \dot{\omega} = [0,0,0]^T$ and $\dot{\phi} = \dot{\theta} = 0$). When considering non-turning steady flight ($\dot{\psi} = p = q = r = 0$), the trim condition constraints simplify to the following set of equations.

$$\bar{X}(\bar{\mathrm{v}},\omega,\bar{R},u) = 0 \quad (11)$$
$$\bar{Y}(\bar{\mathrm{v}},\omega,\bar{R},u) = 0 \quad (12)$$
$$\bar{Z}(\bar{\mathrm{v}},\omega,\bar{R},u) = -ma_g \quad (13)$$
$$L(\bar{\mathrm{v}},\omega,\bar{R},u) = 0 \quad (14)$$
$$M(\bar{\mathrm{v}},\omega,\bar{R},u) = 0 \quad (15)$$
$$N(\bar{\mathrm{v}},\omega,\bar{R},u) = 0 \quad (16)$$

For symmetric aircraft models, and control inputs mirrored about the XZ plane, the constraints may be further reduced to the three longitudinal equations. Since the LA-8 model is not symmetric, all six constraints must be met.

Equilibrium conditions are found by specifying the desired forward and vertical speed, $\bar{u}_0$ and $\bar{w}_0$, then solving for the free variable values that satisfy the nonlinear constraints. In this case, the free variables are the pitch angle, roll angle, and control inputs u. The input vector u, is comprised of the propeller speeds $\omega_p = [\omega_{p_1},\ldots,\omega_{p_8}]^T$, the tilt angle of each wing $\delta_i = [\delta_{i_1},\delta_{i_2}]^T$, the elevon deflections $\delta_e = [\delta_{e_1},\ldots,\delta_{e_4}]^T$, the flap defections $\delta_f = [\delta_{f_1},\ldots,\delta_{f_4}]^T$, and the ruddervator deflections $\delta_r = [\delta_{r_1},\delta_{r_2}]^T$, such that

$$u = \begin{bmatrix} \omega_p^T & \delta_i^T & \delta_e^T & \delta_f^T & \delta_r^T \end{bmatrix}^T. \quad (17)$$

Due to the complexity of the nonlinear equations, solving for the free variables directly requires use of a nonlinear solver. On simpler systems, the Newton-Raphson method can be employed to great effect, but due to the multitude of redundant control effectors of the LA-8, and UAM aircraft in general, the trimming problem is setup as an optimization problem with nonlinear equality constraints

$$\begin{aligned} \min_{\phi\in\Phi,\theta\in\Theta,u\in\mathbb{U}} \quad & J(\phi,\theta,u) \\ \text{subject to} \quad & \bar{X}(\bar{u}_0,\bar{w}_0,\phi,\theta,u) = 0 \\ & \bar{Y}(\bar{u}_0,\bar{w}_0,\phi,\theta,u) = 0 \\ & \bar{Z}(\bar{u}_0,\bar{w}_0,\phi,\theta,u) = -ma_g \\ & L(\bar{u}_0,\bar{w}_0,\phi,\theta,u) = 0 \\ & M(\bar{u}_0,\bar{w}_0,\phi,\theta,u) = 0 \\ & N(\bar{u}_0,\bar{w}_0,\phi,\theta,u) = 0 \end{aligned}, \quad (18)$$

where the cost function $J(\phi,\theta,u)$ may be used to produce a trim condition that, for instance, minimizes the energy usage or maximizes the control authority at that particular flight condition. The optimization problem can be solved with a commercial-off-the-shelf nonlinear programming solver, but it should be noted that the solutions are not unique and depend on where the algorithm is initialized. In this study, the non-turning level flight equilibrium points are presented, but the method can be extended to turning flight with the additional complexity of adding the body angular rates as free variables.

The LA-8 aircraft can be flown in many different ways, so some decisions were made up front for this study. We consider level flight at speeds within in the range of 0-60 ft/s to stay within the bounds of the aerodynamic model. To simplify the optimization problem, the body pitch angle was held at 0°, and the elevons and ruddervators — reserved for control actuation — were set to their neutral positions, $\delta_e = \delta_r = 0°$. The free variables used to trim the aircraft were the roll angle, wing tilt angles, the propeller speeds, and the flaps on both sets of wings. The control effectors were allowed to move independently of one another, i.e., no effectors were ganged together. The cost function used to produce the trim conditions presented in figures 3-5 used a combination of quadratic cost on the usage of the propeller and flaps as well as quadratic cost on the difference between wing tilt angles, propeller speeds, and flap deflections on each wing.

$$\begin{aligned} J = \; & w_1\omega_p^T\omega_p + w_2\delta_f^T\delta_f + w_3(\delta_{i_2}-\delta_{i_1})^2 \\ & + w_4(\delta_{f_2}-\delta_{f_1})^2 + w_5(\delta_{f_4}-\delta_{f_3})^2 \\ & + w_6\sum_{i=1}^{7}(\omega_{p_{i+1}}-\omega_{p_i})^2. \end{aligned} \quad (19)$$

The development of the cost function was the result of an iterative process, of which many combinations of weighting functions and weights were considered. The resulting trim curves were evaluated for relative smoothness and available control authority of the chosen free-variables. The level-flight trim curve presented in figures 3, 4, and 5, show the wing tilt angles, propeller speeds, and flap angles at each trim point for a range of air speeds between 0 and 60 ft/s. The trim curve represents one of many possible solutions.

The wing tilt angles presented in figure 3 show the wing angles decreasing from a trimmed hover condition of approximately 84° and 83° for the forward and rear wing, respectively, down to 11° and 10° at a forward flight speed of 60 ft/s. The wing offset from vertical in hover is expected and is attributed to the need to balance the rear directional lift force generated by the wing in the slipstream of the propeller.

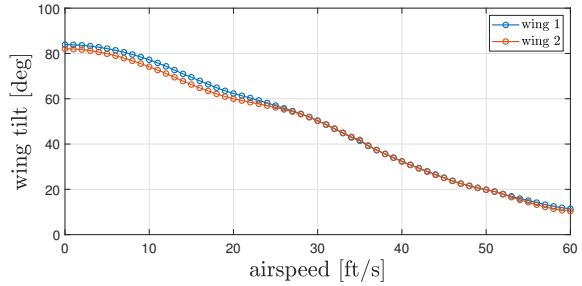

Figure 3. Trim wing tilt angles

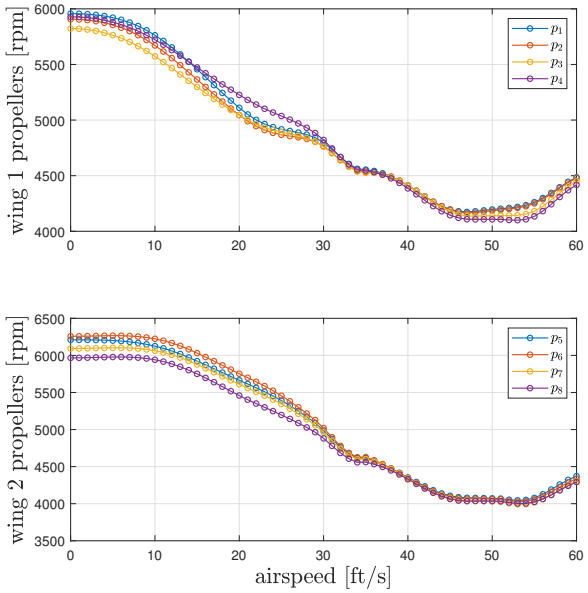

Figure 4. Trim propeller speeds

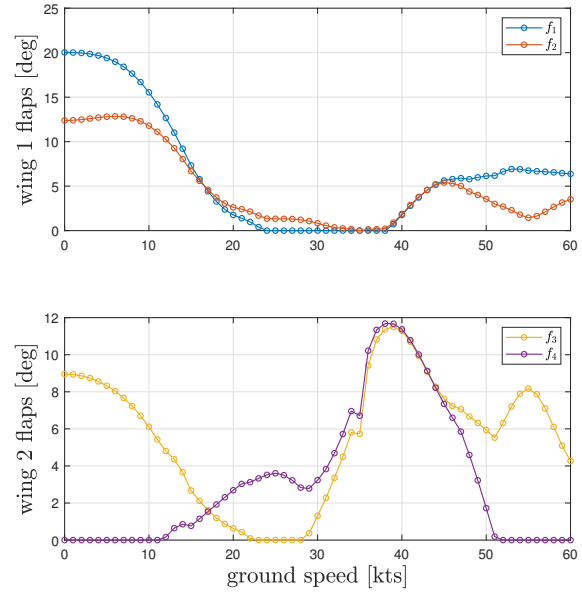

Figure 5. Trim flap deflections

The propeller and flap curves shown in figures 4 and 5 show the need to balance significant asymmetries in the aircraft model. These manifest themselves as both yaw and roll moments in hover where it can be noted that significant differences in flap and propeller speeds are needed when comparing actuation on the left and right side of the aircraft. Flaps 1 and 3 are used to balance out a positive yaw moment while the propellers are used to balance out a negative roll moment.

As the speed is increased, and the wing tilt angle decreased, the asymmetries become less severe between 30 and 45 ft/s ($\approx 50^\circ$ and $\approx 25^\circ$ wing tilt angles), as noted by the decrease in the difference between the left and right control effectors. As the speed is increase beyond 45 ft/s, significant flap differential is needed to balance the roll moment.

The set of trim points form the basis of the transition controller. The dynamics are linearized about a subset of these points, and linear control techniques are employed (described in more detail in the next section) to produce a robust reference-tracking controller. The control gains are scheduled based on the flight speed, and the trim solutions used as feedforward control inputs as the aircraft transitions between flight regimes.

AIRCRAFT CONTROL AUTHORITY

As with many different classes of VTOL aircraft, the LA-8 transitions from thrust-borne flight to lift-borne flight, and in doing so changes how it affects control. Understanding the changing effectiveness of the control actuators, and how much control authority is available as the aircraft traverses the flight envelope is important, since the LA-8 is predominantly open-loop unstable throughout the flight envelope.

To understand how control authority changes, or is transferred between effectors, we look at the linearization of the dynamics at each trim point. From the input Jacobian matrix, insight as to how the effectiveness changes as the aircraft transitions between regimes may be obtained. Additionally, approximations of the total control authority of an individual effector may be produced.

This type of study, following wind tunnel testing and modeling of the aircraft dynamics, can provide early feedback as to how the vehicle is expected to perform and whether or not it can meet the design requirements of the proposed vehicle mission.

The effectiveness and the control authority of the effectors are presented in two plots for each moment direction, i.e., roll, pitch, and yaw. The control effectiveness is presented as a normalized value between -1 and 1, and was obtained by dividing the derivative value in the Jacobian by the absolute value of the maximum derivative value (for that actuator) over all trim points. The control authority of an actuator is approximated by taking the value of the derivative and multiplying it by a nominal change in either direction, taking into account the limits of the actuator by truncating the deflection at the absolute effector limit. The estimated nominal change for each

Table 1. Nominal control deflection

$\Delta\omega_p$	$\Delta\delta_i$	$\Delta\delta_e$	$\Delta\delta_f$	$\Delta\delta_r$
200 RPM	2°	10°	5°	10°

actuator, including propellers, wing-tilt, and surface deflections is listed in Table 1.

Looking first at the pitch moment generation, the actuator effectiveness and control authority can be seen in figures 6 and 7. The top two plots in figure 6 show that the two banks of propellers on the two wings provide opposing pitch moments throughout the transition. In addition, although the effective-

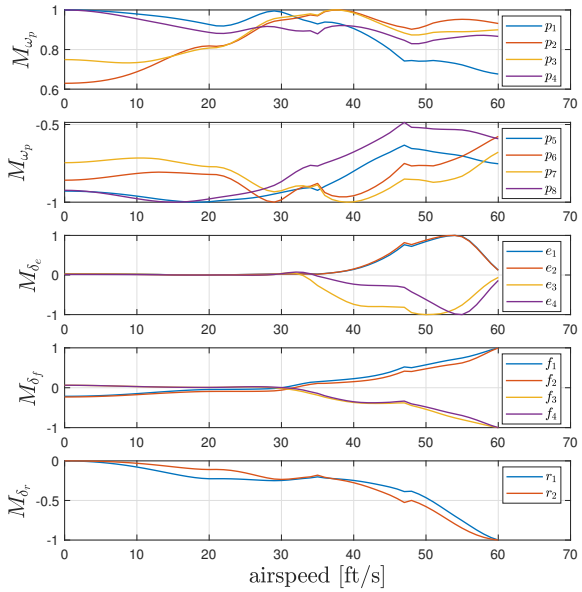

Figure 6. Pitch rate control effectiveness

ness of the propellers is reduced when transitioning to forward flight, the propellers remain a viable means for providing pitch control, due to the vertical offset of the wings relative to the center of mass. The deflecting surfaces (elevons, flaps, and ruddervators), shown in the bottom three plots, do not become effective at generating a pitch moment until there is sufficient dynamic pressure and the wing tilt angle is reduced below 45°. The reduction in the effectiveness of the elevons at high speeds is due to the elevon servo malfunction during wind tunnel testing that was mentioned earlier. The control authority plots in figure 7 reiterate the consistent pitch moment authority of the propeller but show that the deflecting surfaces may provide much more control authority at higher flight speeds. Indeed, if the general quadratic trend that is present in the flaps and ruddervators was reflected in the elevons, it can be expected that the elevons would provide two to three times the pitch moment provided by the propellers in forward flight, possibly at a much lower energy cost. The asymmetric nature of the control authority of flaps 2 and 4 is due to the physical limits of the flap deflections.

Although, in this study, the wing tilt actuator is not used in

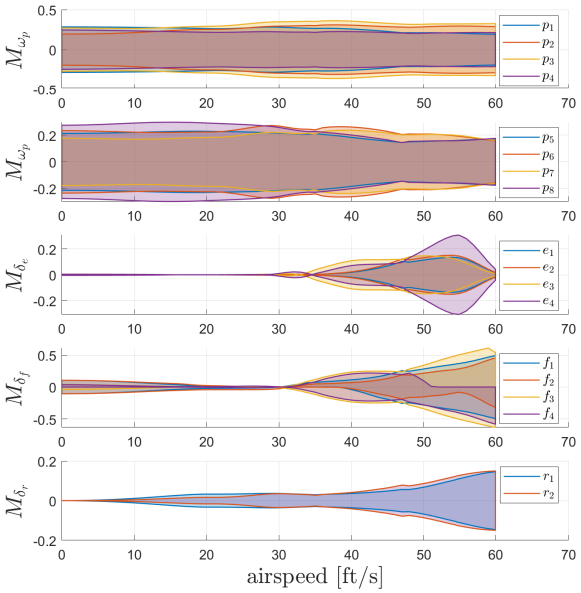

Figure 7. Pitch rate control authority

active feedback control, it is worth noting how the individual tilt of each wing may be used to produce a pitch moment. Figure 8 shows that in hover and lower transition speeds, tilt actuation is not as effective a means with which to produce a pitch moment compared to the propellers, but as the speed is increased and the wing-tilt angles drop below 30° it can be used to great effect.

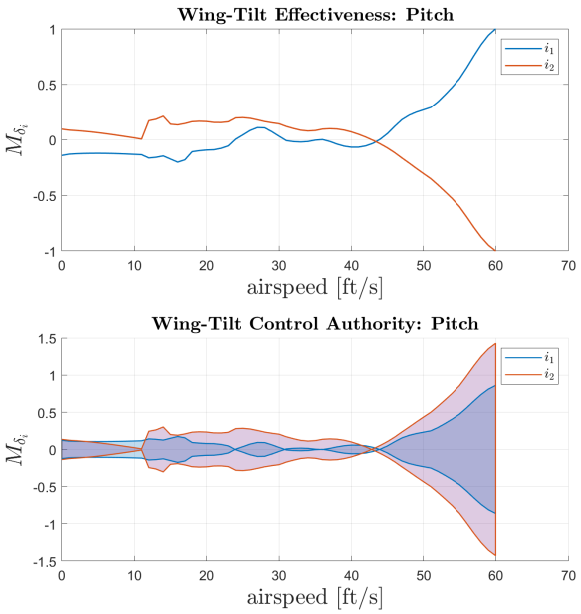

Figure 8. Wing tilt pitch control effectiveness and authority

Moving on to the lateral direction, the roll moment effectiveness and control authority plots are presented in figures 9 and 10 respectively. The effectiveness and control authority

plots show that as the aircraft transitions from hover to forward flight, roll authority is transferred from the propellers to the deflecting surfaces. In both cases, left-right differential actuation may be used to produce a roll moment, and adequate blending of the propellers and surfaces can provide consistent roll authority throughout the transition. The ruddervator surfaces provide little in terms of roll moment production.

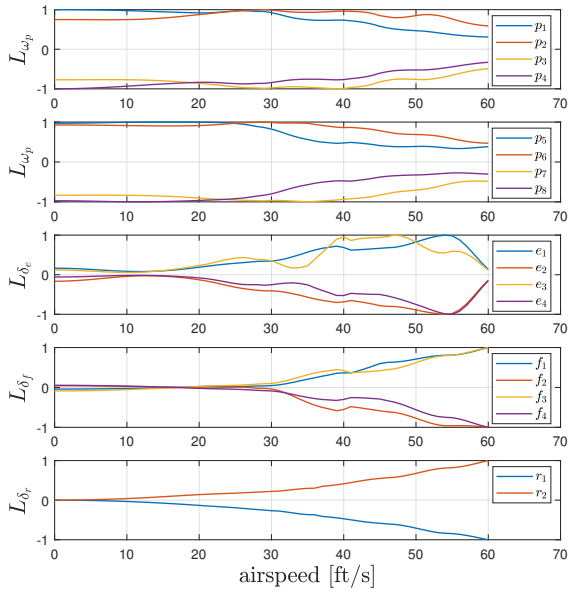

Figure 9. Roll rate control effectiveness

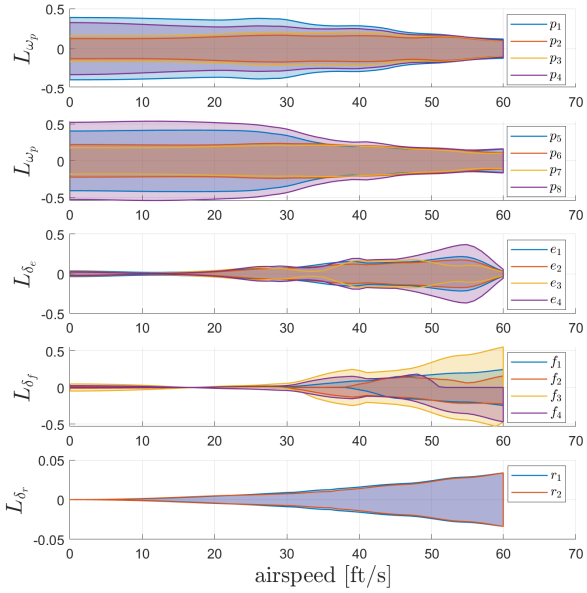

Figure 10. Roll rate control authority

The yaw moment production is particularly interesting, because the propeller yaw moment sign flips during the transition, as seen in figure 11. This phenomenon is due to the

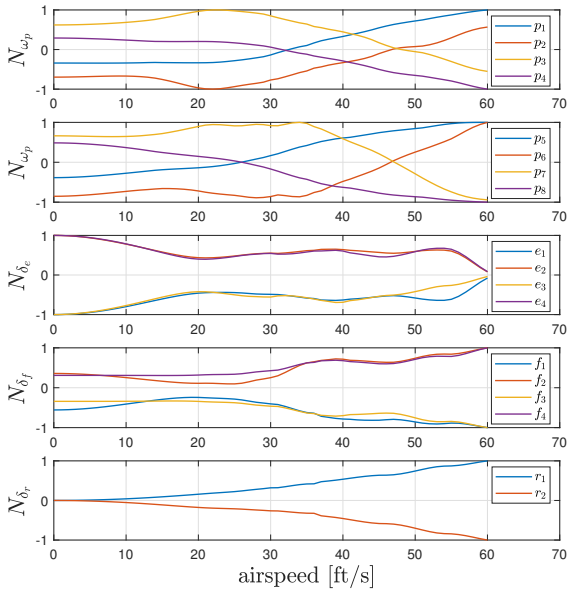

Figure 11. Yaw rate control effectiveness

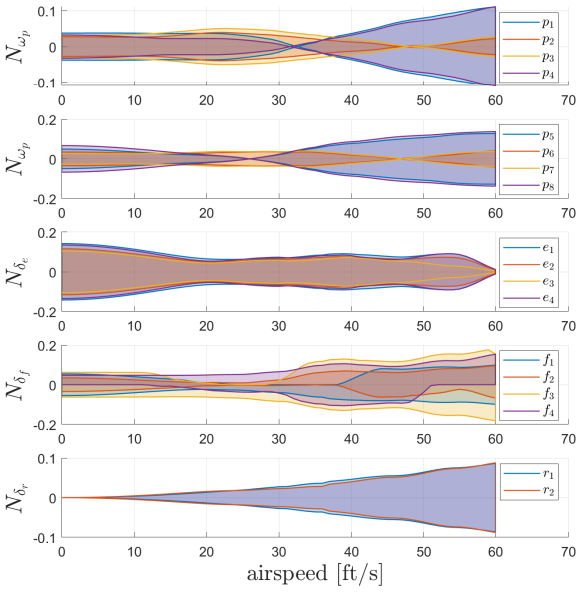

Figure 12. Yaw rate control authority

blown-wing effect in hover, where the local increase in dynamic pressure at the wing due to the propeller slip stream produces a lifting force acting primarily in the direction toward the rear of the aircraft. Figure 12 shows that the outside propellers produce a slightly larger yaw moment in hover. As the wing tilt angle decreases, the yaw moment sign of the propellers switches as the thrust force of the propeller becomes the primary contributor to the yaw moment production.

In hover, the elevons provide the majority of the control authority by directing the slipstream of the propeller and changing the lift production of the wing. As the aircraft transitions, the outside propellers and the ruddervator surfaces provide the

best means of yaw moment production, while the elevons and flaps produce a yaw moment due to the increase/decrease in drag. Use of aerodynamic torque by differentially actuating the clockwise and counter-clockwise propellers, like that of a quad rotor, does not appear to be an effective method of producing yaw as the torque is overpowered by the aerodynamic effects of the blown wing.

As demonstrated by the preceding analysis, the transition of a tiltwing VTOL aircraft is a complex maneuver, in which the changing aerodynamics are compounded by the changing control effectiveness and authority of the control effectors. The saving grace, for the LA-8, lies in the multitude of actuators, where redundancy and overlap provide sufficient control authority throughout the transition. The question remains, how to design a controller that takes into account the dynamic nature of the aircraft and optimizes its usage of the available control effectors at every stage of the transition, while providing safe and reliable trajectory tracking performance.

The next section describes a uniform control architecture that provides a straightforward approach to design a trajectory-tracking controller for transitioning VTOL aircraft.

UNIFORM CONTROL FRAMEWORK

The control structure provides a unified approach to control design throughout the entire flight envelope. This approach brings together several design strategies that are described below to build a method that is applicable across all flight regimes (Ref. 17).

Robust Servo-mechanism Linear Quadratic Regulator

The robust servo-mechanism linear quadratic (RSLQR) structure (Ref. 18) builds on the well-known linear quadratic optimal control theory. When applied to the linearized dynamics of the aircraft at an equilibrium point, the linear quadratic regulator (LQR) forces the system to the origin, forming a type 0 system. When used to track a desired state of the system or reject a constant disturbance, the closed loop response will have a constant steady-state offset, and therefore integral error control action is needed. RSLQR makes use of the internal model principal (Ref. 19), augmenting the state space representation by embedding a model of the class of signals (e.g., step, sinusoidal) to be tracked, then applying optimal control theory. The resulting control structure has two parts: a servo tracking controller for command following and state feedback for stabilization. Together, they provide accurate command tracking and predictable robust performance. In practice, if a constant reference command is sufficient for obtaining the desired performance, then the system type is raised to one, providing zero steady-state error command tracking. This approach has been successfully deployed in many aerospace systems, both autonomous and piloted, and is quickly reviewed here for completeness.

Consider the linear time-invariant system

$$\begin{aligned} \dot{x} &= Ax + Bu, \\ y &= Cx + Du, \end{aligned} \tag{20}$$

where $x \in \mathbb{R}^n$ is the system state, $u \in \mathbb{R}^m$ is the input, and $y \in \mathbb{R}^p$ is a set of outputs. We wish the output, $y(t)$, to track a constant reference signal with zero steady-state error. The error signal is defined by the difference between the reference and the output signal, $e = r - y$. To drive the steady state error to zero, we raise the system type by adding integral action to the error signal, $x_i = -\int e$, and augment the system with this new state:

$$\begin{bmatrix} \dot{x}_i \\ \dot{x} \end{bmatrix} = \begin{bmatrix} 0 & C \\ 0 & A \end{bmatrix} \begin{bmatrix} x_i \\ x \end{bmatrix} + \begin{bmatrix} D \\ B \end{bmatrix} u + \begin{bmatrix} -I \\ 0 \end{bmatrix} r. \tag{21}$$

Taking the derivative of (21) and noting that $\dot{r} = 0$, we arrive at the servo design model

$$\dot{z} = \tilde{A}z + \tilde{B}v, \tag{22}$$

where the design model state vector $z \in \mathbb{R}^{n+p}$ is comprised of the tracking error e and the time derivative of x, and the input $v \in \mathbb{R}^m$ is the time derivative of u, resulting in the state and input vectors $z = [\dot{x}_i, \dot{x}]^T$ and $v = \dot{u}$. The servo design system matrices are defined as

$$\tilde{A} = \begin{bmatrix} 0 & C \\ 0 & A \end{bmatrix}, \quad \tilde{B} = \begin{bmatrix} D \\ B \end{bmatrix}, \tag{23}$$

The tracking controller is obtained by applying the LQR algorithm to (22) using the quadratic cost

$$J = \int_0^\infty z^T Q z + v^T R v \, dt, \tag{24}$$

where $Q = Q^T > 0$, $R = R^T \geq 0$, $(\tilde{A}, \tilde{B})$ is stabilizable, and $(\tilde{A}, Q^{\frac{1}{2}})$ is detectable. The optimal control is $v = -Kz$ where $K = R^{-1}\tilde{B}^T P$, and P is the unique positive definite solution to the algebraic Riccati equation

$$\tilde{A}^T P + P\tilde{A} - P\tilde{B}R^{-1}\tilde{B}^T P = 0, \tag{25}$$

The resulting controller drives the tracking error and the state derivatives to zero but allows the system state to settle in at nonzero values. The design model control, $v = -Kz$, is then integrated to obtain the control input

$$u = -\begin{bmatrix} K_i & K_x \end{bmatrix} \begin{bmatrix} x_i \\ x \end{bmatrix}. \tag{26}$$

where the feedback gain has both integral and proportional components.

The cost function's parameters Q and R are chosen in order to elicit the desired response. A good rule of thumb is to start with weights on just the integrator states. The resultant closed-loop system is shown in Figure 13.

Virtual Controls and Relative Degree

The relative degree of an output to an input is the number of times that output must be differentiated with respect to time such that the derivative is affected directly by that input. For

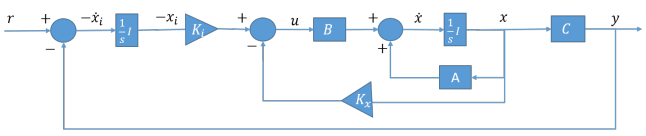

Figure 13. RSLQR control block diagram

example, the vertical velocity of an aircraft in hover has a relative degree of one to the thrust of the rotors, since the thrust of the rotors directly affects the vertical acceleration. On the other hand, in cruise, the relative degree of the vertical velocity to the elevator is two. The elevator input causes a pitch moment which in turn changes the angle of attack increasing the lift production and thus the vertical acceleration.

Virtual controls are introduced to handle the changing relative degree of the aircraft in flight (Ref. 20). The use of virtual controls is analogous to successive loop closure where the feedback loop is closed first on the faster dynamics and time-scale separation of inner and outer loops ensures good overall performance of the system. Here, the use of virtual controls is demonstrated within the RSLQR frame-work using a simplified system representative of a pitch-for-speed type dynamics.

Consider the linear system

$$\begin{aligned} \dot{x}_1 &= ax_3, \\ \dot{x}_2 &= bu, \\ \dot{x}_3 &= x_2. \end{aligned} \tag{27}$$

Expanding into state space gives

$$\begin{bmatrix} \dot{x}_1 \\ \dot{x}_2 \\ \dot{x}_3 \end{bmatrix} = \begin{bmatrix} 0 & 0 & a \\ 0 & 0 & 0 \\ 0 & 1 & 0 \end{bmatrix} \begin{bmatrix} x_1 \\ x_2 \\ x_3 \end{bmatrix} + \begin{bmatrix} 0 \\ b \\ 0 \end{bmatrix} u. \tag{28}$$

Suppose that we would like to use the RSLQR algorithm to track the first two states such that the tracking variables are defined as

$$y = \begin{bmatrix} 1 & 0 & 0 \\ 0 & 1 & 0 \end{bmatrix} \begin{bmatrix} x_1 \\ x_2 \\ x_3 \end{bmatrix}. \tag{29}$$

Using system matrices defined in (28) and (29) and putting them into the servo design model (22), we see that the resulting system is not stabilizable. This is remedied by including the kinematic state x_3 as a virtual control, $\nu = x_3$, and defining a new state vector $\bar{x} = [x_1, x_2]^T$. The resulting design model is then

$$\begin{aligned} \begin{bmatrix} \dot{x}_1 \\ \dot{x}_2 \end{bmatrix} &= \begin{bmatrix} 0 & 0 \\ 0 & 0 \end{bmatrix} \begin{bmatrix} x_1 \\ x_2 \end{bmatrix} + \begin{bmatrix} 0 & a \\ b & 0 \end{bmatrix} \begin{bmatrix} u \\ \nu \end{bmatrix}, \\ y &= \begin{bmatrix} 1 & 0 \\ 0 & 1 \end{bmatrix} \begin{bmatrix} x_1 \\ x_2 \end{bmatrix}. \end{aligned} \tag{30}$$

Applying the RSLQR formulation of Eq. (21) results in the feedback law

$$\begin{bmatrix} u \\ \nu \end{bmatrix} = -K \begin{bmatrix} x_i \\ \bar{x} \end{bmatrix}, \tag{31}$$

where the control gain matrix has the form

$$K = \begin{bmatrix} K_i^u & K_x^u \\ K_i^v & K_x^v \end{bmatrix}. \tag{32}$$

The virtual control is used as a reference for x_3 feedback, and the difference is added to the x_2 reference signal. The design relies on proper time separation of the x_1 and x_2 closed-loop dynamics to ensure good performance, which can be accomplished by weighting the cost matrices Q and R appropriately. The resulting closed loop system is depicted in figure 14, which shows the general structure of the RSLQR with virtual control feedback. The controller dynamics are defined as

$$\begin{aligned} -\dot{x}_i &= r - K_v K_i^v x_i - [K_v K_x^v + K_v C_v + C]x, \\ u &= -K_i^u x_i - K_x^u x, \end{aligned} \tag{33}$$

where, for this particular example, $K_v = [0, 1]^T$ and $C_v = [0, 0, 1]$. For proper dimensions, zeros are appended to the right side of the K_x matrices such that $K_x^v \in \mathbb{R}^{1\times 3}$ and $K_x^u \in \mathbb{R}^{1\times 3}$.

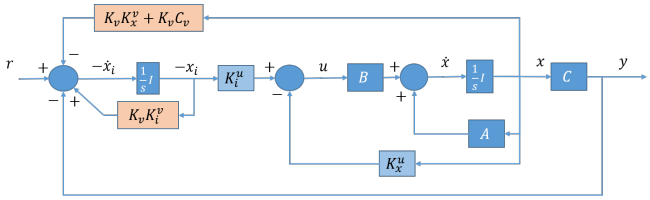

Figure 14. RLSQR with virtual controls

Performance Design and Control Allocation

VTOL aircraft that transition from thrust-borne flight to the more efficient wing-borne flight must traverse a large flight envelope where the effectiveness of a control input may vary greatly, and there are inevitably regions of cross-over where there are multiple effectors capable of producing similar accelerations. To simplify the design process it is helpful to break up the design into two parts: the performance, and the actuation. The performance being the desired response to a command input in any part of the flight envelope, and the actuation pertaining to how the control effort is distributed among the available effectors. This may be accomplished by applying theory presented in (Ref. 21), which is briefly described here for the linear quadratic case.

Consider the linear system

$$\dot{x} = Ax + B_u u, \tag{34}$$

with $A \in \mathbb{R}^{n\times n}$, $B_u \in \mathbb{R}^{n\times m}$, $x(t) \in \mathbb{R}^n$ is the state, and $u(t) \in \mathbb{R}^m$ is the control input. Assume B_u does not have full column rank, implying that it can be factorized as

$$B_u = B_\mu B, \tag{35}$$

where $B_\mu \in \mathbb{R}^{n\times k}$ and $B \in \mathbb{R}^{k\times m}$ both have rank k for some $k < m$. This gives way to an alternative description

$$\begin{aligned} \dot{x} &= Ax + B_\mu \mu, \\ \mu &= Bu, \end{aligned} \tag{36}$$

where $\mu(t) \in \mathbb{R}^k$ may be interpreted as the total control effort of the effectors, most naturally thought of in our application as the total accelerations. Since $k < m$, B and B_u have a non-trivial null space in which u may be perturbed without producing an acceleration μ. Simply put, there are multiple ways to actuate the control input u that produce the same commanded total acceleration μ, and therefore there are built-in redundancies in the control actuation.

When designing optimal feedback control, we explore two approaches. The first poses the optimal control policy in terms of the input u, and the second, poses the optimal control policy in terms of μ, where the solution is then mapped onto u by solving a quadratic optimization problem. We describe the two methods below.

Method 1. Consider the linear system description (34). Determine $u(t)$ by solving

$$\min_{u(t)} \int_0^\infty [x^T Q x + u^T R_u u] dt, \tag{37}$$

where $Q \geq 0$, and $R_u = R_u^T > 0$. This is the standard linear quadratic regulator (LQR) problem. If the pair (A,B_u) is stabilizable and the pair $(A,Q^{\frac{1}{2}})$ is detectable, the optimal control is $u = -R_u^{-1} B_u^T P x$, where P is the unique positive definite solution to the algebraic Riccati equation

$$A^T P + PA - PB_u R^{-1} B_u^T P = 0. \tag{38}$$

Method 2. Consider the linear system description (36). Determine $\mu(t)$ by solving

$$\min_{v(t)} \int_0^\infty [x^T Q x + \mu^T R_\mu \mu] dt, \tag{39}$$

where $Q \geq 0$, and $R_\mu = R_\mu^T > 0$. Again, solving the LQR problem with (A,B_μ) stabilizable and $(A,Q^{\frac{1}{2}})$ detectable, the solution to (39) is $\mu = -R_\mu^{-1} B_\mu^T P x$. Then $u(t)$ is determined by solving

$$\begin{aligned} \min_{u(t)} \quad & u^T W u, \\ \text{subject to} \quad & \mu = Bu, \end{aligned} \tag{40}$$

where $W = W^T > 0$. The solution to this quadratic problem is the weighted generalized inverse $u = W^{-1} B^T (BW^{-1} B^T)^{-1} \mu$.

The main result of (Ref. 21) states that, assuming the matrices R_u and R_μ are related such that $BR_u^{-1} B^T = R_\mu^{-1}$, then u^* and μ^* are the optimal controls associated with design 1 and 2, respectively, and $\mu^* = Bu^*$ and the corresponding trajectories are the same. Further, if for a given R_μ and W the matrix R_u is chosen as $R_u = W + B^T [R_\mu - (BW^{-1} B^T)^{-1}] B$, the control laws for both design methods will be the same.

Thus, by splitting up the control design process, as in method two, the control engineer designs the aircraft response to a command, before determining how that response would be physically implemented via the available effectors. Using general acceleration as inputs alleviates scaling issues that arise when using different types of effectors and helps target specific dynamics that need to be more responsive than others. Once the desired performance is achieved, the second step allows control allocation solutions to be evaluated and tuned using the weighting matrix W. Because the response is the same, provided no effectors are saturated, an apples-to-apples comparison can be made on a per W basis.

LONGITUDINAL CONTROL DESIGN

The uniform control approach described above is applied here to the longitudinal dynamics at a non-turning trim condition. For non-turning flight ($\dot{\psi} = 0$), the longitudinal dynamics simplify to

$$\begin{bmatrix} \dot{\bar{u}} \\ \dot{\bar{w}} \\ \dot{q} \\ \dot{\theta} \end{bmatrix} = \begin{pmatrix} \frac{1}{m} \bar{X}(x_{lon}, u) \\ a_g + \frac{1}{m} \bar{Z}(x_{lon}, u) \\ \frac{1}{J_y} M(x_{lon}, u) \\ q \end{pmatrix}, \tag{41}$$

where the state vector is given by $x_{lon} = [\bar{u}, \bar{w}, q, \theta]^T$, and the input u is the set of effectors listed in eq. (17). Given the trim condition (x_0, u_0) the Jacobian matrices are computed such that

$$A_{lon} = \begin{bmatrix} \frac{1}{m}\bar{X}_{\bar{u}} & \frac{1}{m}\bar{X}_{\bar{w}} & \frac{1}{m}\bar{X}_q & \frac{1}{m}\bar{X}_\theta \\ \frac{1}{m}\bar{Z}_{\bar{u}} & \frac{1}{m}\bar{Z}_{\bar{w}} & \frac{1}{m}\bar{Z}_q & \frac{1}{m}\bar{Z}_\theta \\ \frac{1}{J_y}M_{\bar{u}} & \frac{1}{J_y}M_{\bar{w}} & \frac{1}{J_y}M_q & \frac{1}{J_y}M_\theta \\ 0 & 0 & 1 & 0 \end{bmatrix}, \tag{42}$$

$$B_{lon} = \begin{bmatrix} \frac{1}{m}\bar{X}_{\omega_r} & \frac{1}{m}\bar{X}_{\delta_s} \\ \frac{1}{m}\bar{Z}_{\omega_r} & \frac{1}{m}\bar{Z}_{\delta_s} \\ \frac{1}{J_y}M_{\omega_r} & \frac{1}{J_y}M_{\delta_s} \\ 0 & 0 \end{bmatrix}, \tag{43}$$

where the subscript denotes the variable that the derivative of the force ($\bar{X}$, $\bar{Z}$), or moments (M) is taken with respect to.

As stated previously, the horizontal and vertical velocities ($\bar{u}$,$\bar{w}$) are the variables to be tracked and the pitch rate, q, is to be regulated, which leaves the pitch angle, θ, to be treated as a virtual control input.

The performance design model therefore has states $\bar{x}_{lon} = [\bar{u}, \bar{w}, q]^T$, and the linear design system is

$$\begin{aligned} \dot{\bar{x}}_{lon} &= \bar{A}_{lon} \bar{x}_{lon} + \mu_{lon}, \\ y_{lon} &= \bar{x}_{lon}, \end{aligned} \tag{44}$$

where $\bar{A}_{lon}$ is the upper left 3×3 submatrix of A_{lon} corresponding to the performance states, and μ_{lon} is the general longitudinal control accelerations such that $\mu_{lon} = [\bar{a}_x, \bar{a}_z, \alpha_q]^T$. Applying the RSLQR structure to the system (44), the control design matrices are

$$\tilde{A}_{lon} = \begin{bmatrix} 0 & I \\ 0 & \bar{A}_{lon} \end{bmatrix}, \quad \tilde{B}_{lon} = \begin{bmatrix} 0 \\ I \end{bmatrix}. \tag{45}$$

The components of the Q and R matrices are selected to obtain the desired tracking performance. The desired control accelerations are then

$$\mu_{lon} = -\begin{bmatrix} K_i^{lon} & K_x^{lon} \end{bmatrix} \begin{bmatrix} x_{i_{lon}} \\ \bar{x}_{lon} \end{bmatrix}. \tag{46}$$

The control inputs are determined using the weighted pseudo-inverse

$$\begin{bmatrix} u \\ \theta_{des} \end{bmatrix} = W^{-1}\bar{B}_{lon}^T(\bar{B}_{lon}W^{-1}\bar{B}_{lon}^T)^{-1}\mu_{lon}, \quad (47)$$

where $W = W^T$ is a positive definite weighting matrix, and $\bar{B}_{lon}$ is the input Jacobian augmented with the pitch angle derivatives

$$\bar{B}_{lon} = \left[\begin{array}{cc|c} \frac{1}{m}\bar{X}_{\omega_r} & \frac{1}{m}\bar{X}_{\delta_s} & \frac{1}{m}\bar{X}_{\theta} \\ \frac{1}{m}\bar{Z}_{\omega_r} & \frac{1}{m}\bar{Z}_{\delta_s} & \frac{1}{m}\bar{Z}_{\theta} \\ \frac{1}{J_y}M_{\omega_r} & \frac{1}{J_y}M_{\delta_s} & \frac{1}{m}M_{\theta} \end{array}\right]. \quad (48)$$

The control inputs are executed while the desired pitch angle is fed back, differenced with the measured pitch angle, and used to build the pitch rate reference signal.

Denoting the pseudo inverse matrix $M_{lon} = W^{-1}\bar{B}_{lon}^T(\bar{B}_{lon}W^{-1}\bar{B}_{lon}^T)^{-1}$, it can be decomposed into the submatrices corresponding to the input and pitch angle,

$$M_{lon} = \begin{bmatrix} M_u^{lon} \\ M_\theta \end{bmatrix}. \quad (49)$$

Combining the feedback gains, virtual control, and control allocation, the longitudinal control law is given by the following linear system, (the *lon* subscript is dropped in the interest of space),

$$\begin{aligned} -\dot{x}_i &= -K_\theta M_\theta K_i x_i - (K_\theta M_\theta K_x + K_\theta C_\theta + C)x \\ &\quad + Fr, \\ u &= -M_u(K_i x_i + K_x x), \end{aligned} \quad (50)$$

where $r(t) = [\bar{u}_d, \bar{w}_d]^T$, is the horizontal and vertical velocity commands; F maps the command inputs to the integrated states, and is given by $F = \begin{bmatrix} 1 & 0 & 0 \\ 0 & 1 & 0 \end{bmatrix}^T$; C_θ pulls the pitch angle from the state vector, and is defined as $C_\theta = [0, 0, 0, 1]$; and C selects the tracking states from the state vector, and is defined as

$$C = \begin{bmatrix} 1 & 0 & 0 & 0 \\ 0 & 1 & 0 & 0 \\ 0 & 0 & 1 & 0 \end{bmatrix}.$$

The corresponding block diagram of the controller is shown in figure 15.

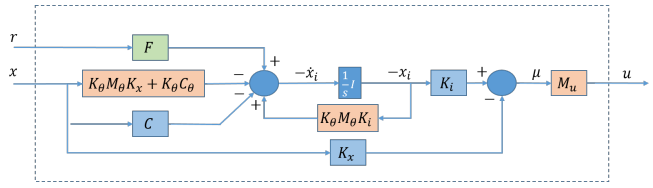

Figure 15. Longitudinal control block diagram

LATERAL CONTROL DESIGN

The lateral dynamics in non-turning flight simplify to the following set of equations

$$\begin{bmatrix} \dot{\bar{v}} \\ \dot{p} \\ \dot{r} \\ \dot{\phi} \end{bmatrix} = \begin{pmatrix} \frac{1}{m}\bar{Y}(x,u) \\ \frac{1}{J_{xz}^2 - J_x J_z}(J_{xz}N(x,u) - J_z L(x_{lat},u)) \\ \frac{-1}{J_{xz}^2 - J_x J_z}(J_x N(x,u) - J_{xz}L(x,u)) \\ p + q\sin\phi\tan\theta + r\cos\phi\tan\theta \end{pmatrix}, \quad (51)$$

where the lateral state vector is given by $x_{lat} = [\bar{v}, p, r, \phi]^T$, and the input u is the set of inputs defined in eq (17). Given the trim condition (x_0, u_0) the state space matrices can be computed and are listed in the appendix.

Of the lateral dynamics, we wish to track the lateral velocity $\bar{v}$ as well as the body roll and yaw rates, p and r. The roll angle, ϕ, is used as virtual control input.

The uniform control design process is then repeated, with the lateral performance model state vector defined as $\bar{x}_{lat} = [\bar{v}, p, r]^T$ and the general control accelerations as $\mu_{lat} = [\bar{a}_y, \alpha_p, \alpha_r]^T$.

Applying the RSLQR algorithm, the lateral integral and state feedback gains, K_i^{lat} and K_x^{lat}, are computed after selecting the appropriate Q and R matrices.

It follows that the control inputs are determined by applying the weighted pseudo-inverse using the roll angle augmented matrix, $\bar{B}_{lat}$, defined in the appendix.

The lateral pseudo-inverse matrix is $M_{lat} = W^{-1}\bar{B}_{lat}^T(\bar{B}_{lat}W^{-1}\bar{B}_{lat}^T)^{-1}$, and can be decomposed into submatrices corresponding to the input and roll angle

$$M_{lat} = \begin{bmatrix} M_u^{lat} \\ M_\phi \end{bmatrix}.$$

The lateral-directional reference commands include the desired lateral velocity in the heading frame, $\bar{v}_d(t)$ and the turn rate $\dot{\psi}_d(t)$, such that the lateral-directional reference is

$$r_{lat}(t) = [\bar{v}_d(t), \dot{\psi}_d(t)]^T. \quad (52)$$

The turn rate command is fed forward, via G in figure 16, to directly command a roll acceleration proportional to the trimmed forward velocity $\bar{u}_0$, and also used to construct the body r reference command. In figure 16 the F and G matrices are defined as

$$F = \begin{bmatrix} 1 & 0 \\ 0 & 0 \\ 0 & 1 \end{bmatrix}, \quad G = \begin{bmatrix} 0 & 0 \\ 0 & \bar{u}_0 \\ 0 & 0 \end{bmatrix}$$

The lateral controller is described mathematically by the following dynamic system in which the *lat* subscript is omitted in the interest of space.

$$\begin{aligned} -\dot{x}_i &= -K_\phi M_\phi K_i x_i - (K_\phi M_\phi K_x + K_\phi C_\phi + C)x \\ &\quad + (F + K_\phi M_\phi G)r, \\ u &= -M_u(K_i x_i + K_x x - Gr). \end{aligned} \quad (53)$$

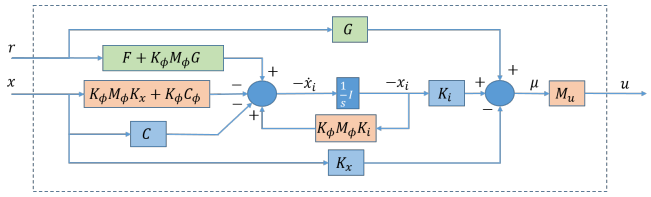

Figure 16. Lateral control block diagram

TRANSITION TRAJECTORY TRACKING

The control architecture is demonstrated by simulating a flight in which the aircraft tracks a desired trajectory. The trajectory, pictured in figure 17, starts in a stationary hover state, begins a vertical ascent, which is followed by a constant radius ascending transition. The aircraft is accelerated to a forward flight speed of 55 ft/s then levels out for a short period at the cruise velocity. The cruise portion of the trajectory is followed by a constant radius helical descent and decelerate to hover.

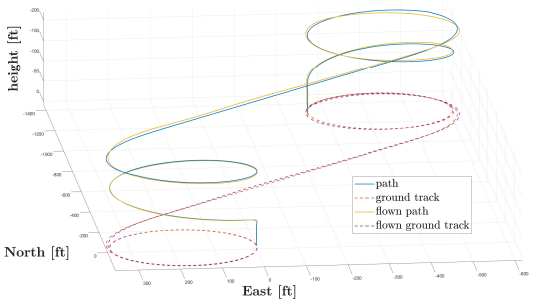

Figure 17. Flight path and ground track of the trajectory

The transition controller is implemented by applying the uniform control architecture at 13 equilibrium points at 5 ft/s increments between 0 and 60 ft/s. The points were taken from the steady level flight trim map described in a previous section.

The control effector weighting matrices were set such that the primary control effectors are the propellers, elevons, and ruddervators, as well as the roll and pitch angle virtual controls. A large weight was placed on the flaps in order to use them as little as possible as control effectors. The weightings were tuned to avoid effector saturation in all flight regimes, which necessitated increasing the weight of the elevons at higher flight speeds due to decrease in the elevon effectiveness represented in the LA-8 aerodynamic model.

The desired forward flight speed was used to schedule the controller gains as well as the feed forward propellers, flaps, and wing tilt angle settings.

The heading frame velocity and turn rate commands are augmented with the position error, expressed in the heading frame, and heading angle error, to more accurately track the inertially referenced trajectory. The complete reference signal going into the longitudinal and lateral controller is

$$r(t) = \begin{bmatrix} \bar{v}_d(t) + K_{\bar{e}}\bar{e}(t) \\ \psi_d + K_\psi e_\psi(t) \end{bmatrix}, \tag{54}$$

where $\bar{e}(t)$ is the inertial position error expressed in the heading frame, $K_{\bar{e}}$ is a tunable feedback gain, and $e_\psi(t)$ is the heading angle error with associated gain K_ψ.

The results of the trajectory tracking simulation are presented in figures 17–22, which show good tracking capabilities in all flight regimes while performing the transition from hover to forward flight and back to hover while climbing, turning and descending. The position error in figure 18 shows a maximum path deviation of 14 ft over the course of the flight, with the largest deviations occurring at the inflection points of the commands.

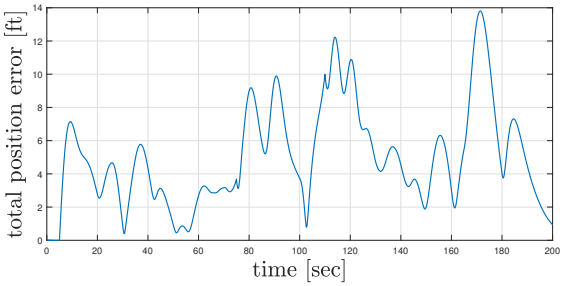

Figure 18. Position error

The heading frame velocity and turn rate commands are presented in figure 19, where it is shown that the scheduled controller sufficiently tracks the command variables as it performs the transition. The largest deviations occur at the inflection points of the commands, most notably, 110 seconds into the simulation where the aircraft begins to descend and decelerate, a known troublesome part of the transition, as any change in wing tilt angle results in large changes in the lifting force generated.

The control actuation throughout the flight is shown in figures 20–22. The speeds of the propellers, which provide lift in hover and thrust in forward flight while also serving as roll, pitch, and yaw effectors in all flight regimes, are shown in figure 20. In figure 21, the control surface actuation is shown, including the wing tilt angles. The wing tilt and flap deflection plots show that they are primarily driven by the trim table schedule, with only slight actuation of the flaps to assist in roll torques in forward flight. This was by design, since the wing tilt was omitted from the control effectors when designing the controller and a large weighting was used to limit the usage of the flaps.

As the aircraft transitions to forward flight, elevons and ruddervators are increasingly used as control effectors. The elevons are used as both roll and pitch effectors, while the ruddervators are used for yaw moment generation. The roll and pitch angles, shown in figure 22, are driven by the controller as virtual controls. The plot shows the roll angle increasing

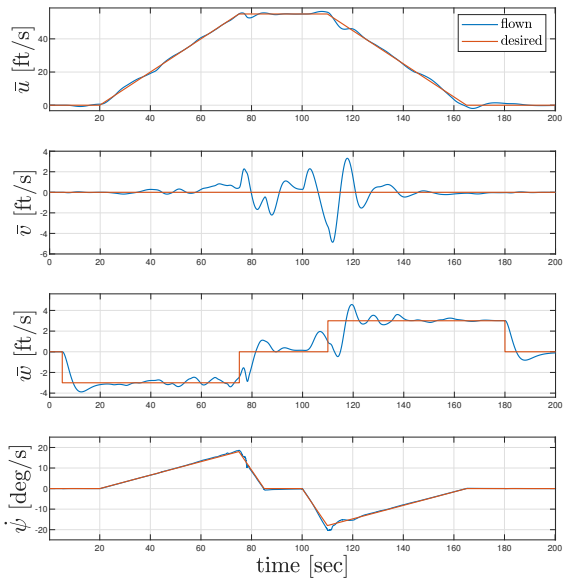

Figure 19. Heading frame command tracking

as the aircraft speed is increased while maintaining the constant radius turn. It then levels off in the cruise portion before increasing in the opposite direction as the aircraft begins its descending transition. The pitch angle is used to decrease the wing angle of attack and point the thrust vector of the propellers forward while accelerating. In the descent, the aircraft is pitched nose up to decelerate.

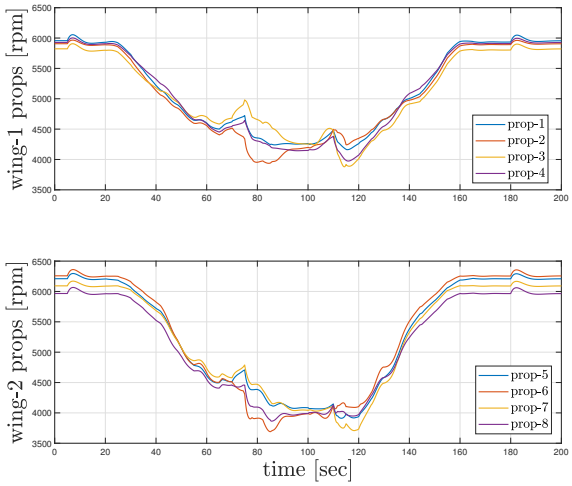

Figure 20. LA-8 propellers speeds

This transition example demonstrates how the relatively simple, robust uniform control approach may be used to pilot a complex aircraft with non-traditional aerodynamics and redundant control effectors through a complex maneuver.

CONCLUSION

We have presented a uniform control architecture that simplifies the control design process of complex vertical take-

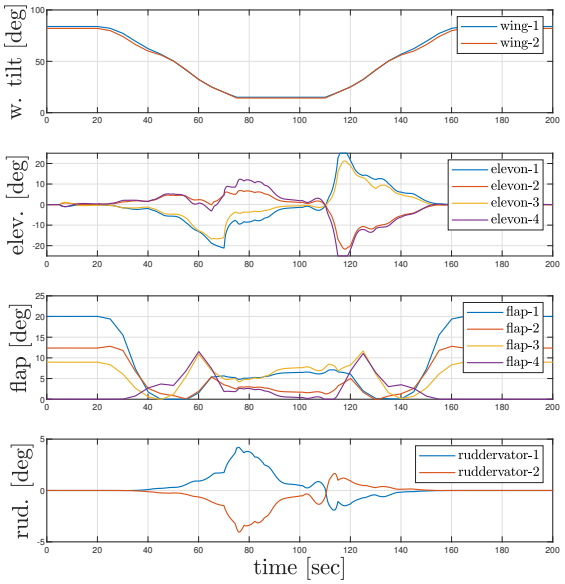

Figure 21. LA-8 control surface deflections

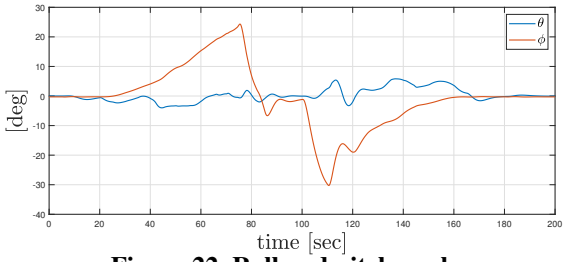

Figure 22. Roll and pitch angles

off and landing aircraft that must transition from thrust-borne flight to lift-borne flight, and, in doing so, must transition between different control effectors. The formulation of the dynamics in the heading frame allows for the use of uniform commands to be used as reference inputs throughout all flight regimes. The uniform framework augments the robust servomechanism linear quadratic control with virtual controls and splits the control design process into the two distinct steps of performance and control allocation. The effectiveness of the control process was demonstrated on a tandem tiltwing distributed electric propulsion VTOL aircraft. The trajectory-tracking simulation results demonstrated that the controller, designed using the robust uniform method, provided accurate trajectory tracking performance while transitioning the aircraft from hover to forward flight and vice versa.

REFERENCES

1. C. Thompson, E. Coleman, and J. Blight, "Integral LQG Controller Design for a Fighter Aircraft," in *Guidance, Navigation and Control Conference*, (Monterey,CA,U.S.A.), American Institute of Aeronautics and Astronautics, Aug. 1987.

2. T. Berger, M. Tischler, S. G. Hagerott, D. Gangsaas, and N. Saeed, "Longitudinal Control Law Design and Handling Qualities Optimization for a Business Jet Flight Control System," in *AIAA Atmospheric Flight Mechanics Conference*, (Minneapolis, Minnesota), American Institute of Aeronautics and Astronautics, Aug. 2012.

3. T. Berger, M. Tischler, S. G. Hagerott, D. Gangsaas, and N. Saeed, "Lateral/Directional Control Law Design and Handling Qualities Optimization for a Business Jet Flight Control System," in *AIAA Atmospheric Flight Mechanics (AFM) Conference*, (Boston, MA), American Institute of Aeronautics and Astronautics, Aug. 2013.

4. D. Gangsaas, J. Hodgkinson, C. Harden, N. Saeed, and K. Chen, "Multidisciplinary Control Law Design and Flight Test Demonstration on a Business Jet," in *AIAA Guidance, Navigation and Control Conference and Exhibit*, (Honolulu, Hawaii), American Institute of Aeronautics and Astronautics, Aug. 2008.

5. P. Hartmann, C. Meyer, and D. Moormann, "Unified Approach for Velocity Control and Flight State Transition of Unmanned Tiltwing Aircraft," in *AIAA Guidance, Navigation, and Control Conference*, (San Diego, California, USA), American Institute of Aeronautics and Astronautics, Jan. 2016.

6. P. Hartmann, C. Meyer, and D. Moormann, "Unified Velocity Control and Flight State Transition of Unmanned Tilt-Wing Aircraft," *Journal of Guidance, Control, and Dynamics*, vol. 40, pp. 1348–1359, June 2017.

7. K. Bordignon and J. Bessolo, "Control Allocation for the X-35B," in *2002 Biennial International Powered Lift Conference and Exhibit*, (Williamsburg, Virginia), American Institute of Aeronautics and Astronautics, Nov. 2002.

8. J. J. Harris, "F-35 Flight Control Law Design, Development and Verification," in *2018 Aviation Technology, Integration, and Operations Conference*, (Atlanta, Georgia), American Institute of Aeronautics and Astronautics, June 2018.

9. S. A. Raab, J. Zhang, P. Bhardwaj, and F. Holzapfel, "Proposal of a Unified Control Strategy for Vertical Take-off and Landing Transition Aircraft Configurations," in *2018 Applied Aerodynamics Conference*, (Atlanta, Georgia), American Institute of Aeronautics and Astronautics, June 2018.

10. P. Bhardwaj, S. A. Raab, J. Zhang, and F. Holzapfel, "Integrated Reference Model for a Tilt-rotor Vertical Take-off and Landing Transition UAV," in *2018 Applied Aerodynamics Conference*, (Atlanta, Georgia), American Institute of Aeronautics and Astronautics, June 2018.

11. J. Zhang, P. Bhardwaj, S. A. Raab, S. Saboo, and F. Holzapfel, "Control Allocation Framework for a Tilt-rotor Vertical Take-off and Landing Transition Aircraft Configuration," in *2018 Applied Aerodynamics Conference*, (Atlanta, Georgia), American Institute of Aeronautics and Astronautics, June 2018.

12. D. D. North, R. C. Busan, and G. Howland, "Design and Fabrication of the LA-8 Distributed Electric Propulsion VTOL Testbed," in *AIAA SciTech Forum*, (VIRTUAL EVENT), American Institute of Aeronautics and Astronautics, Jan. 2021.

13. R. C. Busan, P. C. Murphy, D. B. Hatke, and B. M. Simmons, "Wind Tunnel Testing Techniques for a Tandem Tilt-Wing, Distributed Electric Propulsion VTOL Aircraft," in *AIAA SciTech Forum*, (VIRTUAL EVENT), American Institute of Aeronautics and Astronautics, Jan. 2021.

14. B. M. Simmons and P. C. Murphy, "Wind Tunnel-Based Aerodynamic Model Identification for a Tilt-Wing, Distributed Electric Propulsion Aircraft," in *AIAA SciTech Forum*, (VIRTUAL EVENT), American Institute of Aeronautics and Astronautics, Jan. 2021.

15. B. M. Simmons, "System Identification for Propellers at High Incidence Angles," in *AIAA SciTech Forum*, (VIRTUAL EVENT), American Institute of Aeronautics and Astronautics, Jan. 2021.

16. G. E. Hagen, N. M. Guerreiro, J. M. Maddalon, and R. W. Butler, "An Efficient Universal Trajectory Language," *NASA-TM*, 2017.

17. M. J. Acheson, I. M. Gregory, and J. Cook, "Examination of Unified Control Incorporating Generalized Control Allocation," in *AIAA SciTech Forum*, (VIRTUAL EVENT), American Institute of Aeronautics and Astronautics, Jan. 2021.

18. E. Lavretsky and K. A. Wise, *Robust and Adaptive Control With Aerospace Applications*, ch. 3, pp. 51–70. London: Springer-Verlag, 1 ed., 2013.

19. B. A. Francis and W. M. Wonham, "The Internal Model Principle of Control Theory," *Automatica*, vol. 12, pp. 457–465, 1976.

20. V. S. Akkinapalli and F. Holzapfel, "Incremental Dynamic Inversion based Velocity Tracking Controller for a Multicopter System," in *2018 AIAA Guidance, Navigation, and Control Conference*, (Kissimmee, Florida), American Institute of Aeronautics and Astronautics, Jan. 2018.

21. O. Härkegård and S. T. Glad, "Resolving actuator redundancy—optimal control vs. control allocation," *Automatica*, vol. 41, pp. 137–144, Jan. 2005.

APPENDIX

Lateral Directional State Space Matrices

$$A_{lat} = \begin{bmatrix} \frac{1}{m}\bar{Y}_{\bar{v}} & \frac{1}{m}\bar{Y}_{p} & \frac{1}{m}\bar{Y}_{r} & \frac{1}{m}\bar{Y}_{\phi} \\ \frac{1}{\bar{J}}(J_{xz}N_{\bar{v}} - J_z L_{\bar{v}}) & \frac{1}{\bar{J}}(J_{xz}N_{p} - J_z L_{p}) & \frac{1}{\bar{J}}(J_{xz}N_{r} - J_z L_{r}) & \frac{1}{\bar{J}}(J_{xz}N_{\phi} - J_z L_{\phi}) \\ \frac{-1}{\bar{J}}(J_x N_{\bar{v}} - J_{xz} L_{\bar{v}}) & \frac{-1}{\bar{J}}(J_x N_{p} - J_{xz} L_{p}) & \frac{-1}{\bar{J}}(J_x N_{r} - J_{xz} L_{r}) & \frac{-1}{\bar{J}}(J_x N_{\phi} - J_{xz} L_{\phi}) \\ 0 & 1 & \cos\phi tan\theta & 0 \end{bmatrix}$$

$$B_{lat} = \begin{bmatrix} \frac{1}{m}\bar{Y}_{\omega_p} & \frac{1}{m}\bar{Y}_{\delta_s} \\ \frac{1}{\bar{J}}(J_{xz}N_{\omega_p} - J_z L_{\omega_p}) & \frac{1}{\bar{J}}(J_{xz}N_{\delta_s} - J_z L_{\delta_s}) \\ \frac{-1}{\bar{J}}(J_x N_{\omega_p} - J_{xz} L_{\omega_p}) & \frac{-1}{\bar{J}}(J_x N_{\delta_s} - J_{xz} L_{\delta_s}) \\ 0 & 0 \end{bmatrix}$$

Lateral Directional Control Allocation Matrix

$$\bar{B}_{lat} = \left[\begin{array}{cc|c} \frac{1}{m}\bar{Y}_{\omega_p} & \frac{1}{m}\bar{Y}_{\delta_s} & \frac{1}{m}\bar{Y}_{\phi} \\ \frac{1}{\bar{J}}(J_{xz}N_{\omega_p} - J_z L_{\omega_p}) & \frac{1}{\bar{J}}(J_{xz}N_{\delta_s} - J_z L_{\delta_s}) & \frac{1}{\bar{J}}(J_{xz}N_{\phi} - J_z L_{\phi}) \\ \frac{-1}{\bar{J}}(J_x N_{\omega_p} - J_{xz} L_{\omega_p}) & \frac{-1}{\bar{J}}(J_x N_{\delta_s} - J_{xz} L_{\delta_s}) & \frac{-1}{\bar{J}}(J_x N_{\phi} - J_{xz} L_{\phi}) \end{array}\right]$$